COBEM 2021 26th International Congress of Mechanical Engineering
November 22-26, 2021, Virtual Congress, Brazil

COB-2021-0958
PARAMETRIZATION EFFECT IN RELATION TO MICROHARDNESS, MICROSTRUCTURE AND GEOMETRY OF ROCKIT 401 ALLOY DEPOSITED VIA DIRECTED ENERGY DEPOSITION

Renato Camponogara Panziera
Milton Pereira
Universidade Federal de Santa Catarina (UFSC), Mechanical Engineering Department, Precision Engineering Laboratory (LMP-Laser), Florianópolis, Santa Catarina, Brazil
renato.panziera@hotmail.com, milton.pereira@ufsc.br

Richard de Medeiros Castro
Elvys Isaias Mercado Curi
Flavio Ghedin Neto
Department of Mechanical Engineering, SATC College, Criciúma, SC, Brazil
richard.castro@satc.edu.br, elvys.curi@satc.edu.br, flavio.ghedin@satc.edu.br

Abstract. *The method of deposition of metallic coatings via laser, known as laser cladding, has been used to cover different surfaces and materials in various applications. For each combination of deposited material and substrate, a preliminary study with different parameters of the alloy deposition process is important to study, as these parameters directly influence the mechanical and physical properties of the deposited material. In this work, a study was carried out on the effects that parameterization has in relation to geometry, microstructure, and microhardness of the Rockit 401 metallic alloy deposited via laser Directed Energy Deposition (DED). As a result, it was identified that with the variation of process parameters such as scan speed and power, different bead geometries are obtained, as well as microstructure, and microhardness values. Using the lowest scanning speed of 5 mm/s and low power resulted in higher microhardness values. With increasing power, the alloy's dendritic microstructure presents larger grains, which resulted in a decrease in microhardness. With increasing scan speed, dendritic structures decreased along with microhardness values. Thus, it is clear the importance of tracking the optimized range of the parameters under analysis for each metal alloy.*

Keywords: *coating, laser, parameters, microstructure, microhardness.*

1. INTRODUCTION

Laser cladding can be considered as an additive manufacturing (AM) technique that, by defining the parameters used in the deposit of alloys, gives certain properties for coating components or critical areas of components to improve their functional characteristics. The quality of the coating layer depends directly on the choice of process parameters, the most important being laser power, scan speed, focal length, and powder feed rate (Zhao *et al*., 2018). These are the main parameters that can be commonly changed in a laser deposition process. The selection of optimum deposition parameters is usually based on statistical, analytical, empirical, and numerical simulation methods (Guo *et al.*, 2016) (Yilbas *et al.*, 2012) (Ciubotariu *et al.*, 2016). However, Chen *et al*. (2020), using statistical methods by variance analysis and three-dimensional measurement microscopy, found that the interaction between laser power and powder feed rate directly affect the optimal process parameters. This optimization, promoted for their study, a dense coating, free from cracks, and with low porosity.

Among the various options of powder-based coating techniques, laser metal deposition presents a promising method for the processing of materials, due to its main characteristics: good metallurgical bond with the substrate, greater compaction of the layers, lower coating porosity, low substrate dilution, and low distortion (Hou *et al*., 2018) (Saeedi *et al.*, 2021). Also, according to Gao *et al.* (2019), the deposited Fe-CrNi alloy presented excellent mechanical properties, such as high ductility, good plasticity, as well as good wear resistance, and medium hardness. Other studies demonstrate that the coatings containing elements like Cr, Ni, and Mo improve the mechanical, chemical, and tribological properties of the surfaces of mechanical components (Anjos *et al.*, 1995) (de Sousa *et al.*, 2020). Of the different alloys available, the Rockit 401 is a commercial iron alloy formed by the Fe-CrNiMo elements. Typically, this alloy is used to clad components that require wear resistance and corrosion, such as equipment used in coal mining, where these wear mechanisms act (Ouyang *et al.*, 2021).

The effect of incorrect parameterization directly affects the microhardness, residual stress, and deposited beads geometry (Marzban *et al.*, 2015). The scan speed, power, and spot size parameters are interconnected and directly imply

energy density, thus any difference in any of these parameters means modifications in the microstructure formation. Studies about the incidence of laser thermal load (Nenadl *et al.*, 2014), demonstrate that depending on the used parameters and the material alloy elements, changes in the microstructure are obtained, such as the formation of new phases, altering the hardness, and in some cases the toughness of the material. Increased hardness combined with material ductility also promotes improved tribological performance of contact components (Pirso *et al.*, 2004) (Yang *et al.*, 2003) (Özkavak *et al.*, 2019) (Li and Yang, 2013).

In this study, the behavior of the microstructure, geometry of the beads, and microhardness of the Fe-based coating were evaluated, using the commercial powder Rockit 401, produced by the company Höganäs, whose composition is Fe-18Cr2.5Ni0.5Mo. The microstructural and mechanical properties were evaluated from the deposit of 9 primaries and replicas beads, obtained with different potentials and scanning speeds. The microstructure was obtained by optical microscope (MO) and the microhardness using a Vickers hardness. The assessment was based on the change of scan speeds (v) and laser incidence power (P). These changes, in turn, provided different power densities (E_p), which were correlated with the microhardness, widths (W), heights (h), and depth of penetration (b) of the beads deposited on an AISI 304 stainless steel.

2. MATERIALS AND METHODS

2.1 Raw material and coatings

For the deposition, 304 stainless steel was used as substrate material. Each sample had a dimension of 30 x 30 x 9.53 mm, where six single beads with 26 mm in length each were deposited. Before laser cladding deposition, the samples were blasted with glass spheres for surface cleaning of possible contaminants.

The Rockit 401 commercial powder, from Höganäs manufacturer, was used for single beads depositions. The powder has an apparent density of 3.53 g/cm³. The powder morphology was analyzed by SEM (Figure 1), and showed irregular shape with particle sizes between 53 and 90 µm, as it went through a sieving process with Mesh Tyler 170. The chemical composition of the 304 stainless steel substrate and Rockit 401 powder are shown in Table 1.

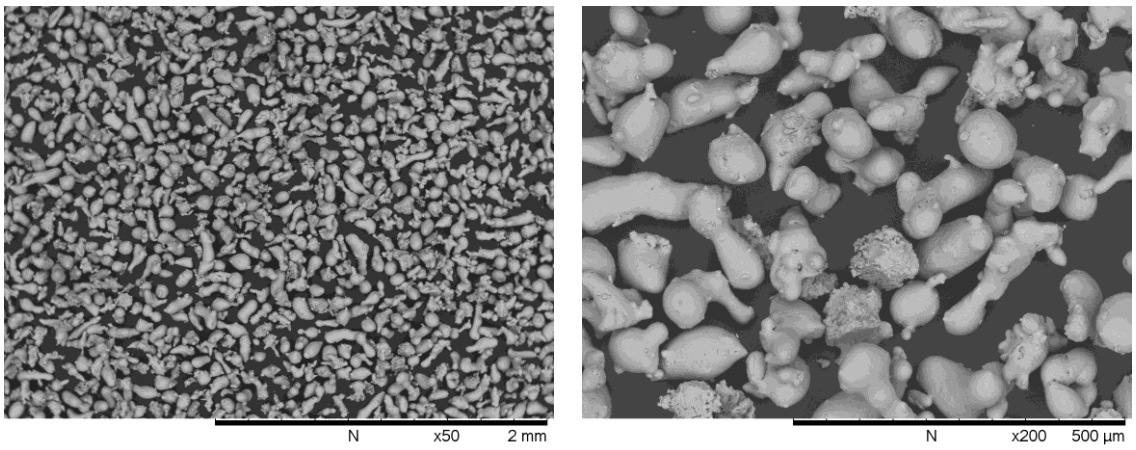

a) b)

Figure 1. SEM images of powder morphology a) and b).

Table 1. Chemical composition of the materials (wt.%).

Materials	Fe	C	Cr	Mo	Ni	Mn	P	S	Si	Others
ABNT 304	Bal.	0.08	18.0 - 20.0	-	8.0 – 10.5	< 2	< 0.045	< 0.030	0.75	
Rockit 401	Bal.	0.15	18	0.5	2.5	-	-	-	-	< 3

2.2 Laser cladding process

To carry out the depositions it was utilized an IPG Photonics® fiber laser source (Yb-Ytterbium), model YLS-10000, with a Precitec optical head, model YW52, a powder nozzle COAX-50-S from Fraunhofer Instituted for Laser Technology (ILT), a GTV Verschleiss-Schutz powder feeding system, and a Siemens SINUMERIK 840D SL Computer Numeric Control (CNC). The system is enabled for 1070–1080 nm wavelength, and operation in continuous mode (CW). The laser optical head, powder nozzle and process chamber are illustrated in Figure 2.

The process parameters for the depositions of the Rockit 401 are presented in Table 2. According to Table 2, laser power varies in 3 and laser scanning speed in 3 different levels, resulting in 9 process parameters. The other process

parameters such as distance between the focal point of the laser beam and the surface - blur in Z (35 mm), spot size (theoretical diameter without blur) 800 μm, carrier gas flow (5.0 L/min – argon gas), shielding gas (15.0 L/min – argon gas) and feed mass flow rate of approximately 7,4 g/min were kept constant. For this powder feed rate the notched disk of the powder feed system operates at 3 RPM. Between the positions of each bead, the substrate temperature was expected to be below 38 ºC.

Through studies carried out by Gutjahr (2016) in this laser equipment, spot sizes of 3.5 mm and 2.5 mm were obtained for blurs of 87.5 mm (Z+ axis) and 47.5 mm (Z+ axis) respectively. The author states that the determination of the focal point position and the respective beam diameters are an approximation based on tests performed on inclined planes where, by trigonometric relations and according to the beam profile "drawn" on a plate, it is possible to infer, in an approximate way, about the diameter of the beam at a given focal distance. It is an alternative and imprecise measure, considering that there is no suitable equipment for the effective characterization of the Laser beam, which is very important for the definition and optimization of parameters for the processes. Therefore, for the 35 mm blur used, it is believed that the diameter of the focal point on the substrate is approximately 1.2 mm.

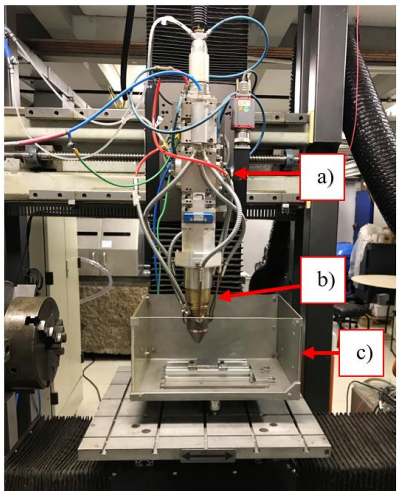

Figure 2. Illustration of the laser optical head (a), powder nozzle (b) and process chamber (c).

Table 2. Process parameters.

Single beads	Laser beam power [W]	Laser beam scanning speed [mm/s]	Diameter spot size [mm]	Power density [J/mm^2]
1	800	5	1.2	133.3
2	800	15	1.2	44.4
3	800	30	1.2	22.2
4	1000	5	1.2	166.7
5	1000	15	1.2	55.6
6	1000	30	1.2	27.8
7	1400	5	1.2	233.3
8	1400	15	1.2	77.8
9	1400	30	1.2	38.9

From the values used for the scanning speed, laser power, as well as the laser beam diameter, the power densities, E_p, (J/mm^2) were estimated. The laser power density is expressed as $E_p = P/(v.d)$, where P is the laser beam power, v is the scanning speed (mm/s) and d is the laser beam diameter, respectively (Cui et al., 2012) (Steen and Mazumder, 2010).

2.3 Caracterization coating

For the microstructural, geometric and morphology characterization of the coating and raw material, the Hitachi scanning electron microscope, model TM3030, with observation condition of 15 kV acceleration voltage and the optical microscope (MO), model Leica DM4000 LED, with DFC 450 camera and software LAS 4.9 were used.

The MO images were obtained from the cross sections of the beads, where the ImageJ software was used to measure the geometric characteristics of all the beads. Figure 3 schematically shows the geometric characteristics of the beads, where height is represented by h, measured from the substrate surface to the top of the bead, bead width represented by

W, penetration depth by b, measured from the substrate surface to the bridge maximum penetration of dilution of the coating on the substrate and finally, wetting angle θ of the beads.

For the microhardness test, the Shimadzu HMV-2T E microhardness tester was used. Ten seconds of loading time were used per measurement with an applied load of 1,961 N in $HV_{0.2}$. For each microhardness profile along the coating depth direction, two repeat tests were performed with 14 indentations each, and the average results of the two repeat tests were used in this article.

The samples were ground on water grinding abrasive paper with grit from 80 to 1200 and finally polished using aluminum oxide suspension with a grain size of 0.3 μm. In order to reveal the coating microstructure on cross section of produced samples, a mixture of 15 ml HCl + 10 ml Glycerol + 5 ml HNO_3 so called glyceregia was used.

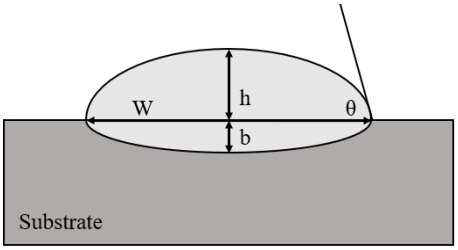

Figure 3. Schematic representation of the geometry of the beads. h is the height, W is the width, b is the depth of penetration of the coating into the substrate and θ the wetting angle of the coating.

3. RESULTS AND DISCUSSION

3.1 Effect of different processing parameters

Figure 4, 5 and 6 show SEM micrographs of cross-sectional beads fabricated by different values of P and v. Visually, the single beads are well bonded to the substrate and were formed at all processing parameters. Through the parameterization used (Table 2), there was little dilution of the coating on the substrate. Table 3 reports the measurement of the geometric characteristics of the primary and replica beads. These measurements were carried out on images obtained by MO as it presents greater contrast between coating and substrate. For the measurements of h, b and W, there is an error between ± 0.01 mm and for θ there is an error between ± 0.2°.

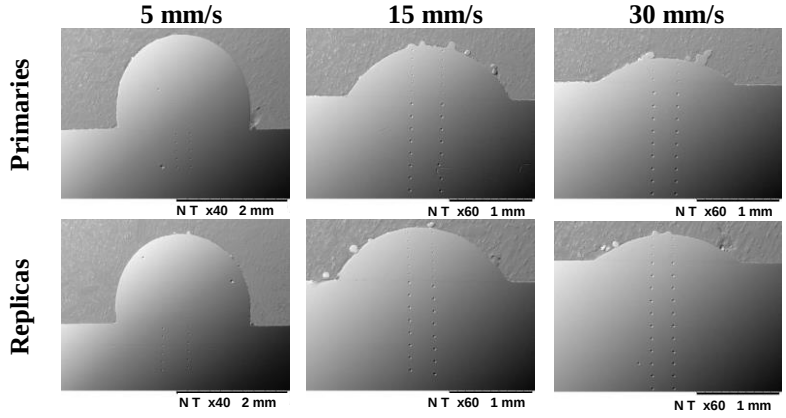

Figure 4. Sem image of single beads samples deposited at different scanning speeds - 800W.

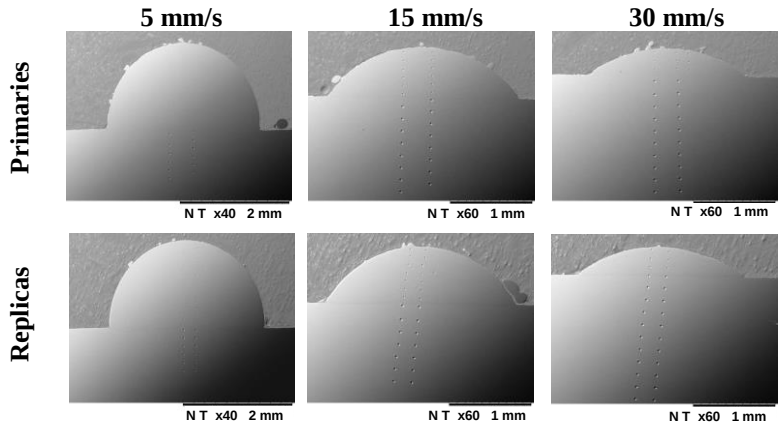

Figure 5. Sem image of single beads samples deposited at different scanning speeds - 1000W.

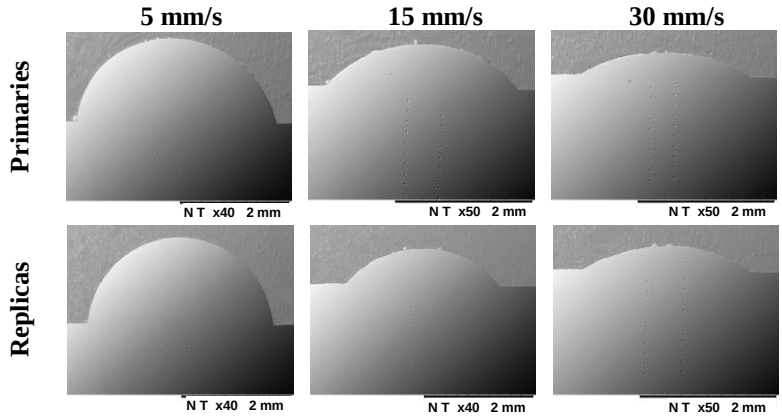

Figure 6. Sem image of single beads samples deposited at different scanning speeds - 1400W.

Table 3. Geometrical properties of the different parameters for Rockit 401 coating.

Geometrical characteristics									
Primaries	h (mm)	b (mm)	W (mm)	θ (°)	Replicas	h (mm)	b (mm)	W (mm)	θ (°)
1	1.643	0.050	2.387	89.70	1	1.731	0.046	2.320	93.80
2	0.633	0.000	1.958	55.00	2	0.642	0.000	2.065	51.00
3	0.297	0.000	1,616	43.60	3	0.328	0.000	1.723	35.30
4	1.601	0.074	2.772	90.00	4	1.627	0.083	2.797	88.00
5	0.619	0.015	2.358	53.60	5	0.685	0.000	2.297	60.10
6	0.332	0.000	1.901	39.50	6	0.349	0.000	1.983	32.93
7	1.529	0.156	3.586	76.10	7	1.592	0.334	3.359	79.01
8	0.616	0.273	2.727	48.90	8	0.650	0.153	2.796	48.20
9	0.319	0.078	2.429	30.30	9	0.351	0.050	2.413	36.00

Figure 7 shows the values of h and b with respect to the scanning speed. It was possible to observe that for the height of the bead, h, both for the primary beads and for the replicas, the values remained close for each power used, as a function of the different scanning speeds. These results are supported by the standard deviation values displayed by the error bar.

In relation to the depth of penetration of the coating on the substrate, b, using the 800 and 1000 W powers, the stability of the primary and replicate beads is also noticeable, unlike the 1400 W power, which showed significant differences in the depth of penetration between beads. This difference between primary and repeatable beads is indicated by the highest values of the standard deviations represented for the three scanning speeds. The same behavior occurred for the wettability angle, θ. This behavior has also been reported by other authors (Tehrani *et al.*, 2020) (Oh *et al.*, 2020) (Jinoop *et al.*, 2019). However, the values obtained for parameter b, show that the scanning speed, as well as the laser power (P), have a great influence on the results, and inversely to those obtained for the bead height. These results can be supported because in this range of power compared to scanning speed, the process of dilution of the beads on the substrate begins, due to the presence of a higher concentration of thermal energy, able to significantly influence this characteristic illustrated by b, beads 7 and 8, in Table 3.

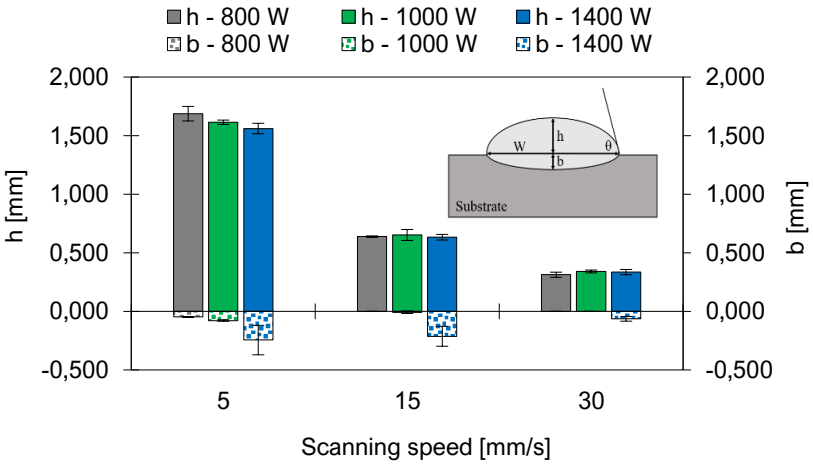

Figure 7. Average and standard deviation of the bead height versus scanning speed in different powers for primary beads and replicas.

When analyzing the bead width (*W*) as a function of scanning speed (Figure 8a-b), it is evident that the bead width presents a linear behavior in relation to the power used, that is, the higher the power, the greater the value of the bead width. This can be analyzed in any power range and scanning speeds for primary beads and replicas. Higher power means the formation of bigger melting pools, which contributes to bigger bead widths. Regarding scanning speed, as the powder feed rate remains the same, lower speeds mean higher powder volume per linear displacement, which contributes to find bigger bead width and height. In Figure 8c, a summary (average) of the primary and replicate beads are shown. The influence of laser power on the bead width of deposited coatings can also be observed. This behavior was also reported by other authors (Tehrani *et al.*, 2020) (Oh *et al.*, 2020) (Jinoop *et al.*, 2019).

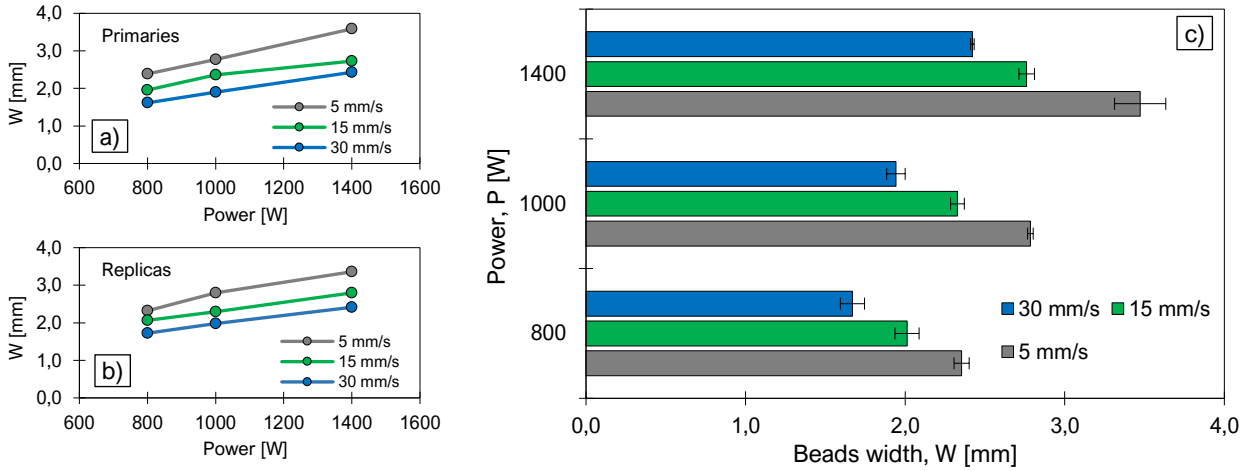

Figure 8. Bead width measurements at different scanning speeds and laser power. (a) primary beads (b) replicate beads and (c) average with one standard deviation of bead width, *W*, relative to the laser power.

3.2 Microstructural evolution during processes

In order to identify potential causes of changes in microhardness values along the cross-section of the deposited beads (section 3.3), the microstructure of the Rockit 401 alloy was analyzed. Figure 9 shows the microstructure of the martensitic matrix with hard eutectic phases of lines 1, 2, and 3 replicates, where: Figures 9a and 9b show the microstructure of bead 1, Figure 9c and 9d the microstructure of bead 2, and Figure 9e and 9f the microstructure of bead 3, with the image of the interface between coating with substrate and the image of the top of the deposited bead, respectively.

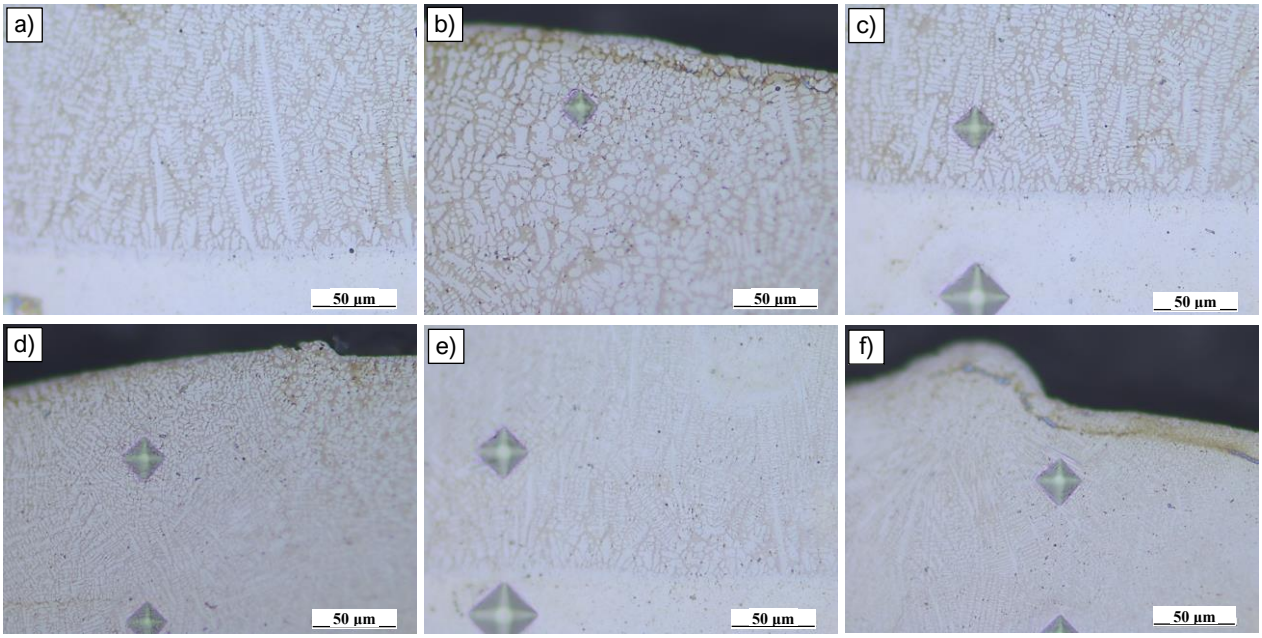

Figure 9. View of the microstructural cross-section of the Rockit 401 alloy from beads 1 (a and b), 2 (c and d) and 3 (e and f) replicates, obtained by MO.

It is possible to notice that in all cases, at the interface of the coating and substrate (Figure 9a, c, and e), the crystal structure presents a dendritic growth with elongated and perpendicular grains with vertical orientation to the top of the coating where there is the greatest dissipation of heat. It also presented a crystal structure with a well elongated primary dendritic arm compared to the secondary dendritic arm. At the top of the cladding there is the presence of disorganized structures with grains hanging from mold and columnar to dendritic in the first tenths of micrometers of the surface. In the center of the beads, the structure remained dendritic for the beads with a scan speed of 30 mm/s and for the other strands there was a mixture between dendritic structures and columnar grains.

With the increase of the scanning speed of 5, 15 and 30 mm/s (Figures 9a and b, c and d, e and f respectively) it is noticed that the size of the dendrites, both in the main and secondary axis, tend to decrease. This is because of the difference in the applied energy and also de difference in the cooling rate experienced by each condition.

All this behavior described in this section remained in the microstructure of beads 4 to 9, proportionally to the increase in laser power when 1000 W and 1400 W were used, that is, the higher the power and the lower the scanning speed, the greater the dendritic structures.

3.3 Microhardness distribution

Due to the large number of primary beads and replicas, it was decided to illustrate the average of the microhardness values performed only in the coatings, the results are shown in Figure 11. However, the microhardness profile of all samples, primary and replicas, consisting of 2 measurements on each bead with 14 indentations each. The highest microhardness values were found when the scanning speed of 5 mm/s was used, later for 15 mm/s and 30 mm/s, as shown in Figure 11a and 11b for primary and replica beads respectively. In all cases the microhardness in the substrate remained at around 200 HV.

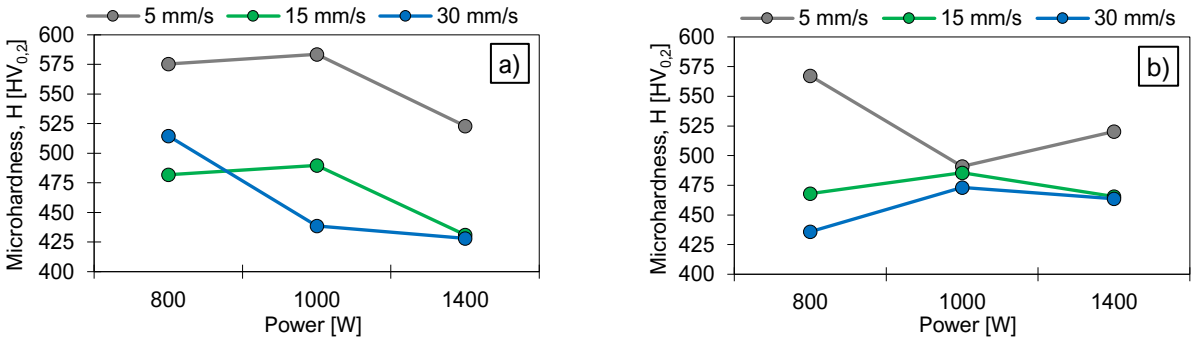

Figure 10. Average microhardness of the coating as a function of power used for primary beads a) and replicas b).

The differences in values found when using a speed of 30 mm/s may have occurred due to these beads having very small geometric values such as h and W, which influences the cooling rate that can change the microstructure of the material, consequently its microhardness in place indentation too close to the surface where the greatest heat extraction occurs. Figures 9e and 9f show that in this range of scan speed the dendritic structures are much smaller compared to the other parameters. Another fact observed is that when analyzing each microhardness profile of the 18 beads separately, the first indentation (farther from the substrate) was the one that presented, in most cases, a higher standard deviation compared to the other indentations. This fact can be explained due to the microstructure difference in the first tenths of micrometers in relation to the surface of the beads as reported in section 3.2, that is, depending on the place of indentation because of changes.

According to Balit, Charkaluk and Constantinescu (2020), in addition to the quality of the sample part, the parameters used in the DED process such as scanning speed, power used, powder flow and scanning strategy are the main parameters that drive the growth of the microstructure and, therefore, control the properties mechanics. Still, according to the authors one can remark an epitaxial growth of elongated grains from the interface and oriented towards the center of the deposited track. Moreover, one can also observe the presence of small grains located close to the surface in contact with the air. Figure 12 shows the microhardness profiles, as well as a summary of the average microhardness as a function of the different power densities. The 14 points of the microhardness profile in Figure 12 illustrate an indication of the indentation position in the beads, thus, it does not have a necessarily equal depth relationship between the samples, but only an indication of position to determine the behavior of the studied parameters.

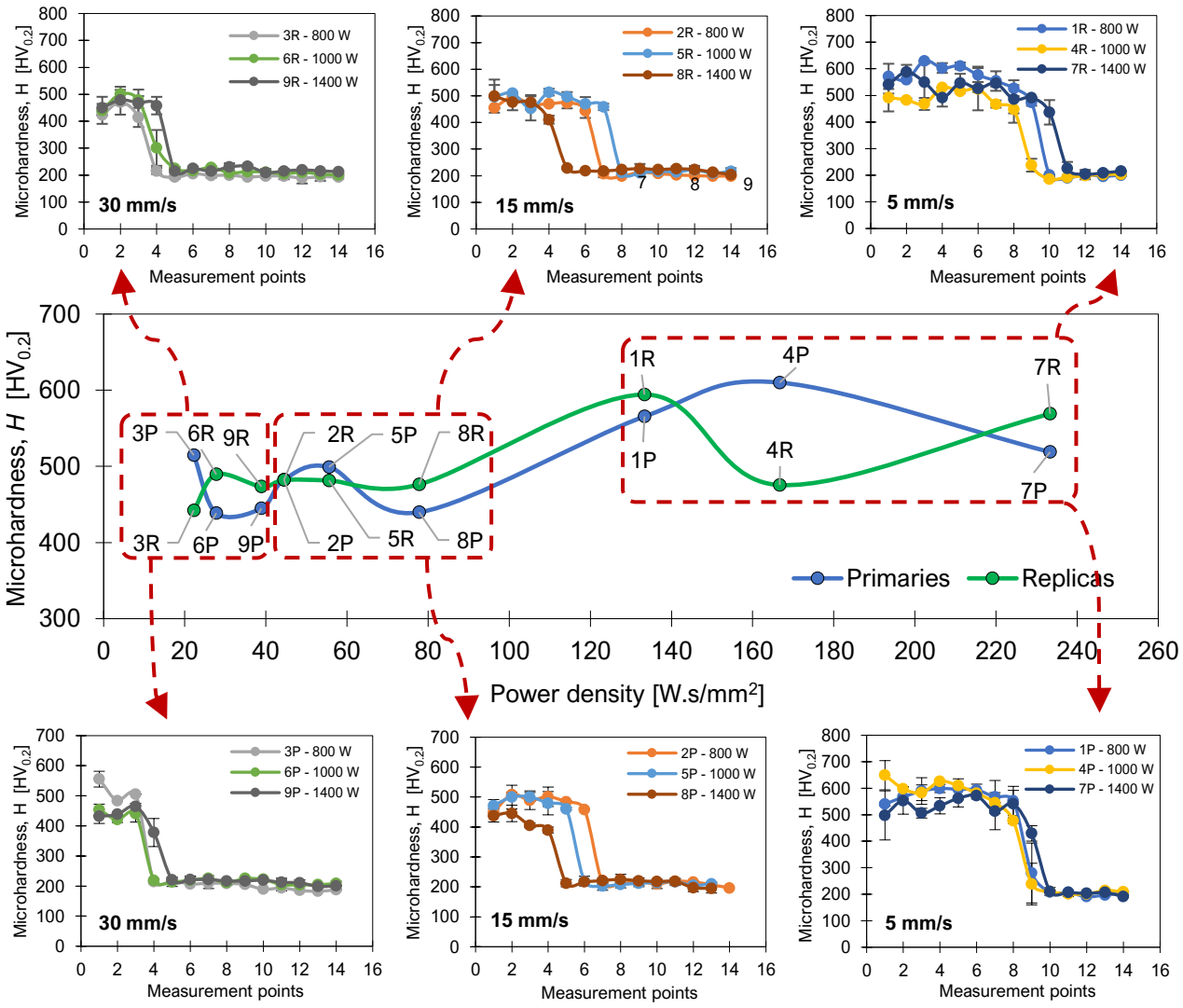

Figure 11. Microhardness profile of the cross-section of the primary beads and replicates and average values for each power density.

The microhardness analysis as a function of the speed and depth of the bead is observed as follows: In Figure 12 (replica beads - R) with the highest scanning speed (30 mm/s), three points were obtained that are between 400 to 500 $HV_{0.2}$, with similar behaviors in the microhardness distribution. The three points of greater microhardness highlighted are due to the smaller heights of the cord and that had similar dimensions. This occurred for all samples of the different applied powers. At half the scan speed (15 mm/s), the highest power of 1400 W had 4 microhardness points just above 400 $HV_{0.2}$, while at the 1000 and 800 W powers, 5 to 6 points stood out of microhardness, close to 500 $HV_{0.2}$, and with similar behaviors between them. At the lowest scanning speed (5 mm/s), no less than 8 microhardness points were obtained above 500 $HV_{0.2}$ and close to 600 $HV_{0.2}$, with a gradual drop in microhardness towards the substrate.

The ratio of the mean microhardness (microhardness versus power density) of the first three measurement points allows for better visualization of the results. It is observed that the beads executed with the highest scanning speed (30 mm/s) correspond to the lowest power density values. It is noticed that all points (3P, 6P, 9P, 3R, 6R and 9R) were below 40 J/mm^2. In these cases, the microhardness mean behavior had variability, being above 400 $HV_{0.2}$ and close to 500 $HV_{0.2}$, both for the primary beads and their replicas.

For the scan speed of 15 mm/s, the power density was between 40 and 90 J/mm^2, with coincidence between the 2P and 2R points, and with the microhardness close to 500 $HV_{0.2}$ at the power of 800 W. With the power of 1000 W, the 5P and 5R points were close, being these with an average of 500 $HV_{0.2}$. At the power of 1400 W, which corresponds to 8P and 8R, the values were variable and the average was a little lower than the previous results.

For a scan speed of 5 mm/s, power density between 130 and 240 J/mm^2, at points 1P and 1R, the microhardness was close to 600 $HV_{0.2}$, using 800 W, showing a slight variability. With 1000 W, the 4P and 4R points are far apart, at these points their average microhardness is close to 500 $HV_{0.2}$. At 1400 W power, which corresponds to 7P and 7R, the values were also variable, with microhardness close to 1000 W power.

4. CONCLUSIONS

Single beads with Rockit 401 alloy were deposited on a 304 stainless steel substrate via laser cladding. In this study, a series of experiments were carried out to explore the microstructure, microhardness, and geometry of the beads through different process parameters. The main conclusions are listed below.

With the increase of the laser power used, the width W of the beads increased for all the scanning speed ranges. The same was not observed for the height h of the beads, which remained practically constant with the increase in the power used when comparing the variations in scanning speed.

The microstructure of the beads presented a martensitic matrix with hard eutectic phases with a predominance of dendritic grains. With increasing power, dendritic grains increased proportionally, and with increasing scanning speed, the grains decreased. The region of the top of the beads presented a variation in the first tenths of micrometers, leaning from columnar to dendritic grains towards the substrate. This phenomenon influenced the microhardness in this indentation region.

The highest values of microhardness were found in the parameter of lower power and lower scan speeds. With the increase in the scanning speed, there was a decrease in the microhardness of the beads.

5. ACKNOWLEDGEMENTS

This research was funded by the Research and Innovation Support Foundation of Santa Catarina State - FAPESC, Brazil, via the project identified by FAPESC, nº 06/2019 - Valorização do Carvão Mineral. The project is intituled as: aumento da eficiência das brocas de perfuração e rotores de bombas centrífugas usando revestimentos resistentes ao desgaste visando o crescimento econômico das mineradoras de carvão, and is coordinated by the researcher, Dr. Ing. Elvys Isaías Mercado Curi.

6. REFERENCES

Anjos, M. A., Vilar, R., Li, R., Ferreira, M. G., Steen, W. M., and Watkins, K., 1995. "Fe-Cr-Ni-Mo-C alloys produced by laser surface alloying". *Surface and Coatings Technology*, Vol. 70, No. 2-3, pp. 235-242.

Balit, Y., Charkaluk, E., and Constantinescu, A., 2020. "Digital image correlation for microstructural analysis of deformation pattern in additively manufactured 316L thin walls". *Additive Manufacturing*, Vol. 31, pp. 100862.

Chen, Y., Wang, X., Zhao, Y., Song, B., and Yu, T., 2020. "Interactive optimization of process parameters and coating analysis of laser cladding JG-3 powder". *The International Journal of Advanced Manufacturing Technology*, pp. 1-11.

Ciubotariu, C. R., Frunzăverde, D., Mărginean, G., Șerban, V. A., and Bîrdeanu, A. V., 2016. "Optimization of the laser remelting process for HVOF-sprayed Stellite 6 wear resistant coatings". *Optics & Laser Technology*, Vol. 77, pp. 98-103.

Cui, C., Ye, F., and Song, G., 2012. "Laser surface remelting of Fe-based alloy coatings deposited by HVOF". *Surface and Coatings Technology*, Vol. 206, No. 8-9, pp. 2388-2395.

de Sousa, J. M. S., Ratusznei, F., Pereira, M., de Medeiros Castro, R., and Curi, E. I. M., 2020. "Abrasion resistance of Ni-Cr-B-Si coating deposited by laser cladding process". *Tribology International*, Vol. 143, pp. 106002.

Gao, W., Chang, C., Li, G., Xue, Y., Wang, J., Zhang, Z., and Lin, X., 2019. "Study on the laser cladding of FeCrNi coating". *Optik*, Vol. 178, pp. 950-957.

Guo, H. F., Tian, Z. J., and Huang, Y. H., 2016. "Laser surface remelting of WC–12Co coating: finite element simulations and experimental analyses". *Materials Science and Technology*, Vol. 32, No. 8, pp. 813-822.

Gutjahr, J., 2016. Desenvolvimento e implementação de um sistema CNC, modular e reconfigurável, para processos LASER. Master's Thesis, Graduate Program in Mechanical Engineering, Federal University of Santa Catarina, Florianópolis, Brazil.

Hou, X., Du, D., Wang, K., Hong, Y., and Chang, B., 2018. "Microstructure and wear resistance of Fe-Cr-Mo-Co-CB amorphous composite coatings synthesized by laser cladding". *Metals*, Vol. 8, No. 8, pp. 622.

Jinoop, A. N., Paul, C. P., Mishra, S. K., and Bindra, K. S., 2019. "Laser Additive Manufacturing using directed energy deposition of Inconel-718 wall structures with tailored characteristics". *Vacuum*, Vol. 166, pp. 270-278.

Li, C. J., and Yang, G. J., 2013. "Relationships between feedstock structure, particle parameter, coating deposition, microstructure and properties for thermally sprayed conventional and nanostructured WC–Co". *International Journal of Refractory Metals and Hard Materials*, Vol 39, pp. 2-17.

Marzban, J., Ghaseminejad, P., Ahmadzadeh, M. H., and Teimouri, R., 2015. "Experimental investigation and statistical optimization of laser surface cladding parameters". *The International Journal of Advanced Manufacturing Technology*, Vol. 76, No. 5-8, pp. 1163-1172.

Nenadl, O., Ocelík, V., Palavra, A., and De Hosson, J. T. M., 2014. "The prediction of coating geometry from main processing parameters in laser cladding". *Physics Procedia*, Vol. 56, pp. 220-227.

Oh, W. J., Son, Y., Cho, S. Y., Yang, S. W., Shin, G. Y., and Shim, D. S., 2020. "Solution annealing and precipitation hardening effect on the mechanical properties of 630 stainless steel fabricated via laser melting deposition". *Materials Science and Engineering: A*, Vol. 794, pp. 139999.

Ouyang, C., Bai, Q., Yan, X., Chen, Z., Han, B., and Liu, Y., 2021. "Microstructure and Corrosion Properties of Laser Cladding Fe-Based Alloy Coating on 27SiMn Steel Surface". *Coatings*, Vol. 11, No. 5, pp. 552.

Özkavak, H. V., Şahin, Ş., Saraç, M. F., and Alkan, Z., 2019. "Comparison of wear properties of HVOF sprayed WC-Co and WC-CoCr coatings on Al alloys". *Materials Research Express*, Vol. 6, No. 9, pp. 096554.

Pirso, J., Letunovitš, S., and Viljus, M., 2004. "Friction and wear behaviour of cemented carbides". *Wear*, Vol. 257, No. 3-4, pp. 257-265.

Saeedi, R., Razavi, R. S., Bakhshi, S. R., Erfanmanesh, M., and Bani, A. A., 2021. "Optimization and characterization of laser cladding of NiCr and NiCr–TiC composite coatings on AISI 420 stainless steel". *Ceramics International*, Vol. 47, No. 3, pp. 4097-4110.

Steen, W. M., and Mazumder, J., 2010. *Laser material processing*. Ed. springer science & business media.

Tehrani, H. M., Shoja-Razavi, R., Erfanmanesh, M., Hashemi, S. H., and Barekat, M., 2020. "Evaluation of the mechanical properties of WC-Ni composite coating on an AISI 321 steel substrate". *Optics & Laser Technology*, Vol. 127, pp. 106138.

Yang, Q., Senda, T., and Ohmori, A., 2003. "Effect of carbide grain size on microstructure and sliding wear behavior of HVOF-sprayed WC–12% Co coatings". *Wear*, Vol. 254, No. 1-2, pp. 23-34.

Yilbas, B. S., and Akhtar, S. S., 2012. "Laser re-melting of HVOF coating with WC blend: Thermal stress analysis". *Journal of Materials Processing Technology*, Vol. 212, No. 12, pp. 2569-2577.

Zhao, Y., Guan, C., Chen, L., Sun, J., and Yu, T., 2020. "Effect of process parameters on the cladding track geometry fabricated by laser cladding". *Optik*, Vol. 223, pp. 165447.

7. RESPONSIBILITY NOTICE

The authors are the only responsible for the printed material included in this paper.